Effect of grain size on mechanical characteristics and work-hardening behavior of fine-grained Mg-0.8Mn alloy via adjusting extrusion temperature

C.C. Li [a,b], X.G. Qiao [a], W.T. Sun [a,g*], I.S. Golovin [e,f], H.S. Kim [b, c,d**], Taku Sakai [h], M.Y. Zheng [a, *]

[a] School of Material Science and Engineering, Harbin Institute of Technology, Harbin 150001, PR China

[b] Graduate Institute of Ferrous & Eco Materials Technology, Pohang University of Science and Technology (POSTECH), Pohang, 790794, South Korea

[c] Institute for Convergence Research and Education in Advanced Technology, Yonsei University, Seoul, 03722, South Korea

[d] Advanced Institute for Materials Research (WPI-AIMR), Tohoku University, Sendai, 980-8577, Japan

[e] Department of Physical Metallurgy of Non-Ferrous Metals, National Research Technological University "MISiS", Leninskii pr. 4, Moscow 119049, Russia

[f] Moscow Polytechnic University, B. Semenovskay 38, Moscow, 107023 Russia

[g] School of Engineering, Lancaster University, Lancaster, LA14YW, UK

[h] The University of Electro-Communications, Chofu, Tokyo 182-8585, Japan

* Corresponding author. E-mail address: zhenghe@hit.edu.cn (M.Y. Zheng); hskim@postech.ac.kr (Hyoung Seop Kim); sunwt_hit@126.com (W.T. Sun)

Abstract

In this study, the Mg-0.8Mn (M08, wt.%) alloy is subjected to hot extrusion at various temperatures ranging from 150 °C to 300 °C, and the correlations between the microstructure evolution, tensile properties, and work hardening behavior at ambient temperature are elaborated. The M08 alloy extruded at 150 °C exhibits a bimodal microstructure, which included undynamic recrystallized (unDRXed) grains and fine dynamic recrystallized (DRXed) grains with an average size of 1.4 μm. As the extrusion temperature exceeds 210 °C, fully DRXed grains can be observed with grains growth becoming more pronounced with the increase of extrusion temperature. Notably, Mn atomic segregations are evident at the grain boundaries (GBs) in the M08 alloy extruded at 150 °C. It is also essential to highlight that the propensity for GB segregation is diminished with higher extrusion temperature, and the amount of α-Mn precipitates within grain interiors is increased in the M08 sample extruded at 300 °C. An intriguing observation is the abnormal rise in yield strength (YS) with grain size as the extrusion temperature is increased. This phenomenon can be attributed to the diminishing effect of GB sliding and the concurrent enhancement of GB strengthening effect. However, as the extrusion temperature is raised from 150 °C to 300 °C, the ductility of M08 alloy experiences a substantial decline from 74% ± 4% to 16% ± 3%. Meanwhile, the grain growth can bring about an increased strain hardening rate, which is primarily dependent on the transition in the dominant deformation mechanism from grain boundary sliding (GBS) to dislocation slip. This transition leads to a more substantial accumulation of dislocations within the coarser grains, thereby affecting the mechanical behavior of M08 alloy. This work provides valuable insights into the influence of extrusion temperature on the microstructure evolution and mechanical properties of Mg-0.8Mn alloy, offering a foundation for optimizing the processing parameters to achieve desired mechanical performance.

***Keywords**:* Mg-Mn alloy; DRXed grain size; Mechanical property; Grain boundary segregation; Work hardening behavior

1. Introduction

The ongoing advancements in industrial manufacturing have heightened the demand for lightweight materials to realize the reduction in energy consumption and carbon emissions[1–3]. Among the potential candidates, magnesium (Mg) alloys are particularly noteworthy because of their high strength-to-weight ratio, making them ideal for various structural applications requiring lightweight properties [4]. Despite these advantages, Mg alloys is usually constrained by their inherently low ductility at ambient temperatures. This limitation is primarily derived from their hexagonal close-packed (HCP) crystal structure, which restricts the availability of slip systems, thus cannot satisfy the von Mises criterion for sufficient plastic deformation in polycrystals [5]. Accordingly, the enhancement in the comprehensive mechanical properties of Mg alloys is crucial for expanding their practical use in the industrial fields.

Recent studies have demonstrated that microalloying and grain refinement are two effective strategies for enhancing the ductility and work-hardening behavior of Mg alloys[6]. For instance, the introduction of microalloying elements such as manganese (Mn) has been adopted to reduce stacking fault energy (SFE) and critical resolved shear stress (CRSS) of non-basal slip systems, thus promoting the activation of additional slip systems at room temperature and consequently enhancing ductility[7–9]. A comparative study on as-extruded Mg-xCa/Mn/Ce alloys and pure Mg highlighted the role of these elements in grain refinement and texture modification, which directly improved the ultimate tensile strength and elongation[8]. Meanwhile, incorporating the alloying elements is conducive to promote grain boundary sliding (GBS) in fine-grain Mg alloys at ambient temperature, which contributes to the enhanced ductility. Besides, controlling the grain size through thermomechanical processing techniques like extrusion has emerged as a key method for improving the overall plastic deformation of Mg alloys, and the resultant grain refinement is beneficial for promoting the prismatic and pyramidal slips, which are typically challenging to activate in coarse-grained materials [10,11].

Another critical factor influencing the mechanical behavior of Mg alloys is GBS, which becomes a dominant deformation mechanism under high-temperature conditions, typically higher than $0.5T_m$ (T_m: melting temperature) [12]. Studies on pure Mg [13], Mg-Mn [14], Mg-Bi [15]and Mg-Li [16] alloys with ultrafine grains have demonstrated that grain refinement can activate GBS at lower temperatures, significantly improving ductility even at room temperature[17,18]. For example, the fine-grained pure Mg with a mean grain size of 1.3 μm revealed that the plastic deformation was primarily accommodated through GBS, rather than dislocation activity within individual grains [19]. This verifies the synergistic effect of GBS and grain rotation in reducing stress concentration and enhancing ductility. Additionally, the Mg-0.3 Mn (at.%) binary alloy subjected to hot extrusion processing exhibited an average grain size of 2.5 μm., and the post-deformation microstructural observations revealed that the fracture was predominantly initiated from the cavitation associated with GBS instead of deformation twinning, resulting in a high strain rate sensitivity (*m*-value) ranging from 0.06 to 0.22 [20]. Similarly, high-pressure torsion processing of Mg-8Li (wt.%) alloy achieved remarkable room-temperature superplasticity of approximately 440 %, with around 60 % of the total elongation deriving from the enhanced GBS. The increase of GBS was attributed to the rapid diffusion along grain boundaries (GBs, which was facilitated by Li atomic segregation and the formation of Li-rich interphases[21].

Owing to their HCP crystal structure, Mg alloys are typically characterized by limited ductility and pronounced work hardening rates (θ) at room temperatures[22]. The mechanical performance of Mg alloys, such as strength, ductility and deformability, are intricately related to work hardening behavior. This work hardening behavior is mainly determined by the grain size and its distribution, which can regular the response of materials to deformation processes[23,24]. For example, the impact of microstructure on the strain rate sensitivity (SRS) was explored in AZ31 Mg alloy, and the reduced grain size can cause a substantial increase in SRS, particularly below 15 μm. This enhanced SRS was found to be strongly correlated with strain hardening, revealing that finer grains tend to decrease the work hardening rate at ambient temperatures, contrary to conventional predictions[25]. Moreover, after equal-channel angular extrusion followed by annealing, the AZ31B Mg alloy exhibited substantial elongation of 47% during tensile testing at room temperature. The fine grain structure was critical in activating non-basal slip systems and promoting dynamic recovery, which not only improved ductility but also potentially influenced the work hardening rate [26]. This evidence underscores the importance of microstructural control in improving both the strength and ductility of Mg alloys. Therefore, controlling grain size and optimizing GB conditions are essential to affect the deformation modes and improve the comprehensive mechanical response.

In our previous study, a detailed analysis was conducted to understand the influence of Mn content on the microstructural characteristics and mechanical behavior of Mg-Mn alloys processed by extrusion. Specifically, the Mg-0.8 wt.% Mn (M08) alloy, characterized by a bimodal structure comprising fine dynamic recrystallized (DRXed) grains of approximately 2.3 μm and elongated unDRXed regions, demonstrated exceptional ductility at room temperature. This superior ductility can be attributed to the effective interaction of GBS within the fine-grained microstructure, which is enhanced by the presence of α-Mn nano-precipitates at GBs[27]. Building upon this, the current work further explores the impact of extrusion temperature on grain refinement, grain boundary segregation and precipitation behavior in the as-extruded M08 alloy. By systematically varying the extrusion temperature, the purpose is to elucidate how these microstructural changes can affect the mechanical properties, particularly focusing on the work-hardening behavior and ductility during tensile deformation. It can provide an in-depth understanding of the relationship between extrusion temperature, grain size, mechanical behavior and work-hardening response of fine-grained Mg-0.8Mn (wt.%) alloy. Through the controlled adjustment of extrusion conditions, this work seeks to address the limitations posed by the inherently poor ductility of Mg alloys at room temperature. The findings are expected to contribute to refining extrusion processing techniques to achieve superior mechanical performance in Mg-0.8Mn (wt.%) alloys, particularly in applications requiring enhanced ductility at room temperature.

2. Experimental section

The Mg-0.8Mn (wt.%) alloy, denoted as M08, was produced through permanent mold direct-chill casting using commercially pure Mg and a Mg-3.2Mn (wt.%) master alloy. The actual chemical composition was determined as Mg-0.81Mn (wt.%) by inductively coupled plasma (ICP) mass spectrometry. The ingots underwent a homogenization treatment at 510 °C for 12 h, and then placed in warm water at 50 °C to cool down. Direct extrusion was performed at a ram speed 0.1 mm/s at various temperatures of 150 °C, 180 °C, 210 °C, 250 °C and 300 °C, respectively (in order to simplify, the samples were named as M08-150, M08-180, M08-210, M08-250, and

M08-300, respectively). The extrusion ratio was set as 12.

The microstructural features of the as-extruded M08 alloys were examined using a scanning electron microscope (SEM, ZEISS Supra 55 SAPPHIRE) fitted with an electron backscattered diffraction (EBSD) detector, as well as a transmission electron microscope (TEM, Talos F200X). Specimens for EBSD analysis were polished by SiC sandpaper to #4000, and then electrolytic polishing was used until the surface was like a mirror. Finally, the argon ion polishing was used to remove the surface stress. The EBSD step size was set as 0.4 μm, and the acceleration voltage was 20 kV. EBSD data were analyzed using Channel 5 software. A grain orientation spread (GOS) of 1° was employed as a standard threshold to differentiate between DRXed) and unDRXed grains.

The mechanical properties of the as-extruded M08 alloys were assessed using an Instron-5569 testing apparatus at ambient temperature, and the strain rate was set as 1 $x10^{-3}$ s^{-1}. Tensile test samples, featuring a gauge length of 15 mm and a cross-sectional area of 6×2 mm^2, were cut from the extrusion rods oriented along the extrusion direction (ED). The tensile yield strength and ultimate tensile strength were determined using the 0.2% offset method, in accordance with the ASTM E8 standard [28]. A Young's modulus of 45 GPa, corresponding to that of pure Mg [5], was employed for calculating the strengthening contributions from structural factors. This is due to the minimal effect of the microalloying addition of Mn on the Young's modulus of Mg. To ascertain the SRS (m-value) of the M08 alloy after hot extrusion, nanoindentation creep tests were performed using a Berkovich tip with an applied load of 500 mN. The tests involved a constant loading and unloading rate of 50 μN/s and a hold period of 500 s.

3. Results and Analysis

3.1 Microstructure characteristics of different as-extruded M08 alloys

Fig. 1 presents the inverse pole figure (IPF) maps of M08 alloy extruded at various temperatures, with the observations taken along ED. It is evident from the IPF maps that the unDRXed regions contain amount of low angle grain boundaries (LAGBs). Typically, when the extrusion temperature does not exceed 210 °C, the as-extruded M08 alloy exhibits a bimodal microstructure consisting of fine DRXed grains and elongated coarse grains. As shown in Fig. 1(a-c), the volume fractions of DRXed grains in the as-extruded M08 alloy at extrusion temperatures of 150 °C, 180 °C, and 210 °C are estimated to be 80.7%, 90.8%, and 95.1%, respectively. Moreover, the average sizes of the DRXed grains at these temperatures are measured to be 1.4 ± 0.1 μm, 2.3 ± 0.2 μm, and 2.9 ± 0.2 μm, respectively. When the extrusion temperature exceeds 250 °C, a completely DRXed microstructure can be obtained. Specifically, after extrusion at 250 °C and 300 °C, the average DRXed grain sizes of M08 samples are determined to be 2.9±0.2 μm and 4.9±0.3 μm, respectively. These observations suggest a direct relationship between the extrusion temperature, the extent of dynamic recrystallization, and the grain size in the as-extruded M08 alloy. Fig. 1(f) shows the variation in grain size and the fraction of low-angle grain boundaries (LAGBs) with extrusion temperature, respectively. The volume fraction of LAGBs in the as-extruded M08 alloy with a bimodal microstructure is 20.7%, which is decreased to 14.8% in the M08-300 sample with a fully DRXed structure.

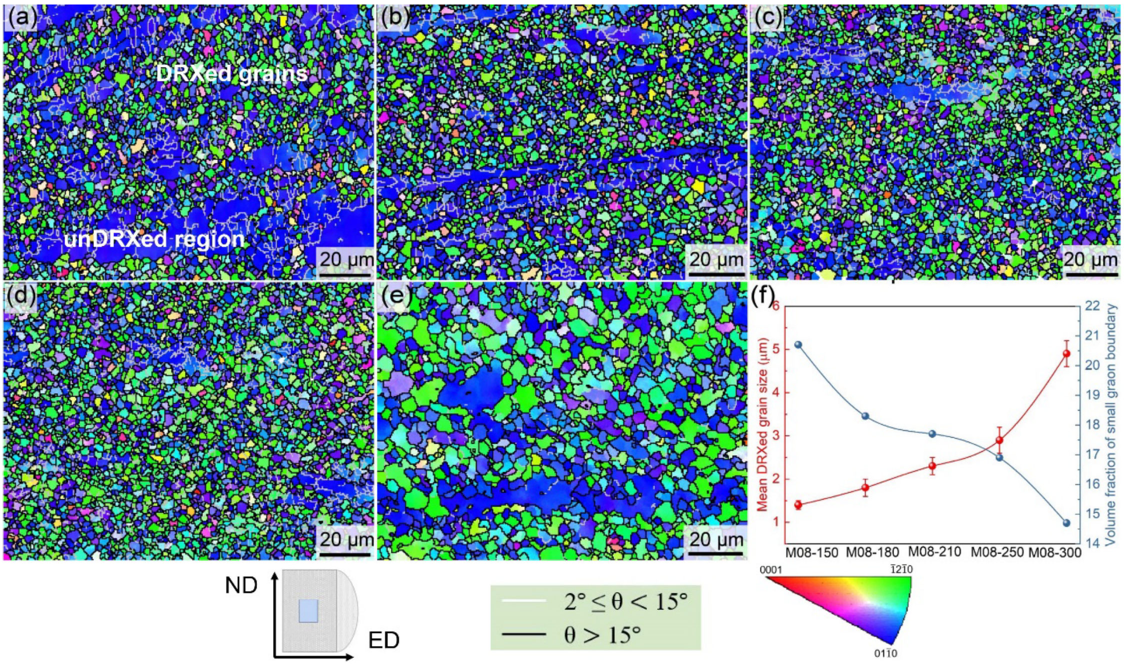

Fig. 1. IPF maps of the Mg-0.8Mn alloy extruded at various temperatures: (a) 150 ℃; (b) 180 ℃; (c) 210 ℃; (d) 250 ℃; (e) 300 ℃; (f) Histogram of grain size distributions and fraction of low-angle grain boundary in as-extruded M08 sample with the variation of extrusion temperatures.

Fig. 2 shows IPF images taken from the different microstructural regions, including both fully DRXed and unDRXed areas of the as-extruded M08 alloy with various temperatures. All the as-extruded M08 alloys present typical fiber texture with {0001} planes and <01$\bar{1}$0> directions parallel to the ED. As illustrated in Fig. 2 (a), the M08-150 sample possesses a bimodal structure, which exhibits a texture intensity of 3.98 within the DRXed region and 22.22 within the unDRXed region. As compared to the M08-150 sample, the texture intensity in the DRXed regions of M08-210 alloy is increased to 4.47, while in the unDRXed regions, it is diminished to 12.75 (Fig 2(c)).

Despite the increase in extrusion temperature from 150 °C to 300 °C, the overall texture type remains unchanged. Besides, the basal texture intensity in the DRXed regions shows an upward trend as the extrusion temperature rising, which is probably ascribed to the preferential growth of DRXed grains [29].

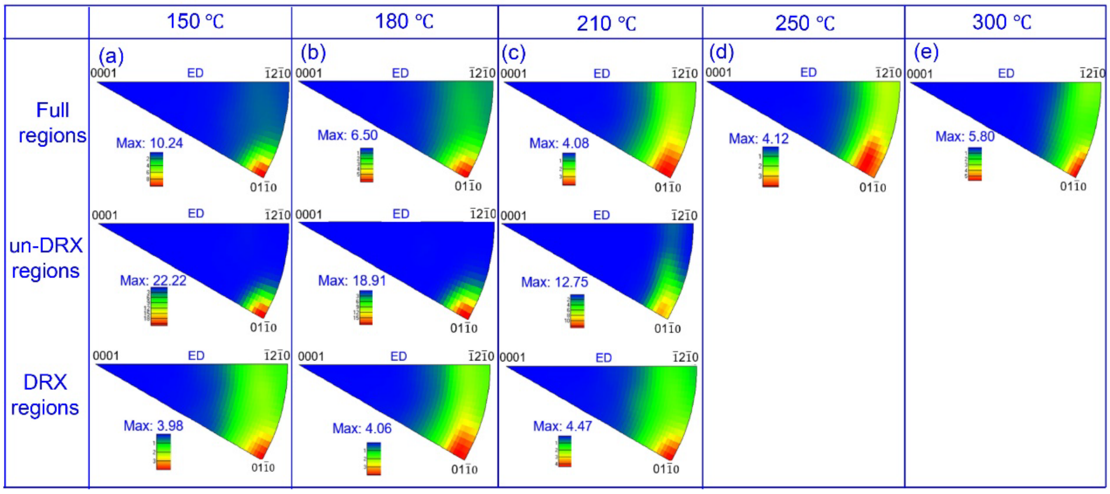

Fig. 2 IPF figures from Full regions, un-DRXed regions, DRXed regions of the as-extruded Mg-0.8Mn alloy with different temperature: (a)150 °C, (b) 180 °C, (c) 210°C, (d) 250 °C and (e) 300 °C.

Fig. 3 shows the SEM images of different as-extruded M08 samples. Fig. 3(f) shows the changes in volume fraction and particle size distribution of precipitates as the extrusion temperature increasing. Obviously, the precipitates in M08-150 alloy exhibit an average particle size of 0.4±0.03 μm, whereas in the M08-300 alloy, the mean particle size of precipitates is increased to 0.8±0.04 μm. It should be noted that the proportion of precipitates is increased with the rise in extrusion temperature. The measured volume fractions of precipitates in the M08 samples extruded at 150 °C, 180 °C, 210 °C, 250 °C and 300 °C are 0.05%, 0.12%, 0.27%, 0.33% and 0.38%, respectively. These results demonstrate an obvious positive correlation between the extrusion temperature, the particle size and volume fraction of precipitates, suggesting that higher extrusion temperatures can facilitate the growth and increased density of precipitates within the α-Mg matrix.

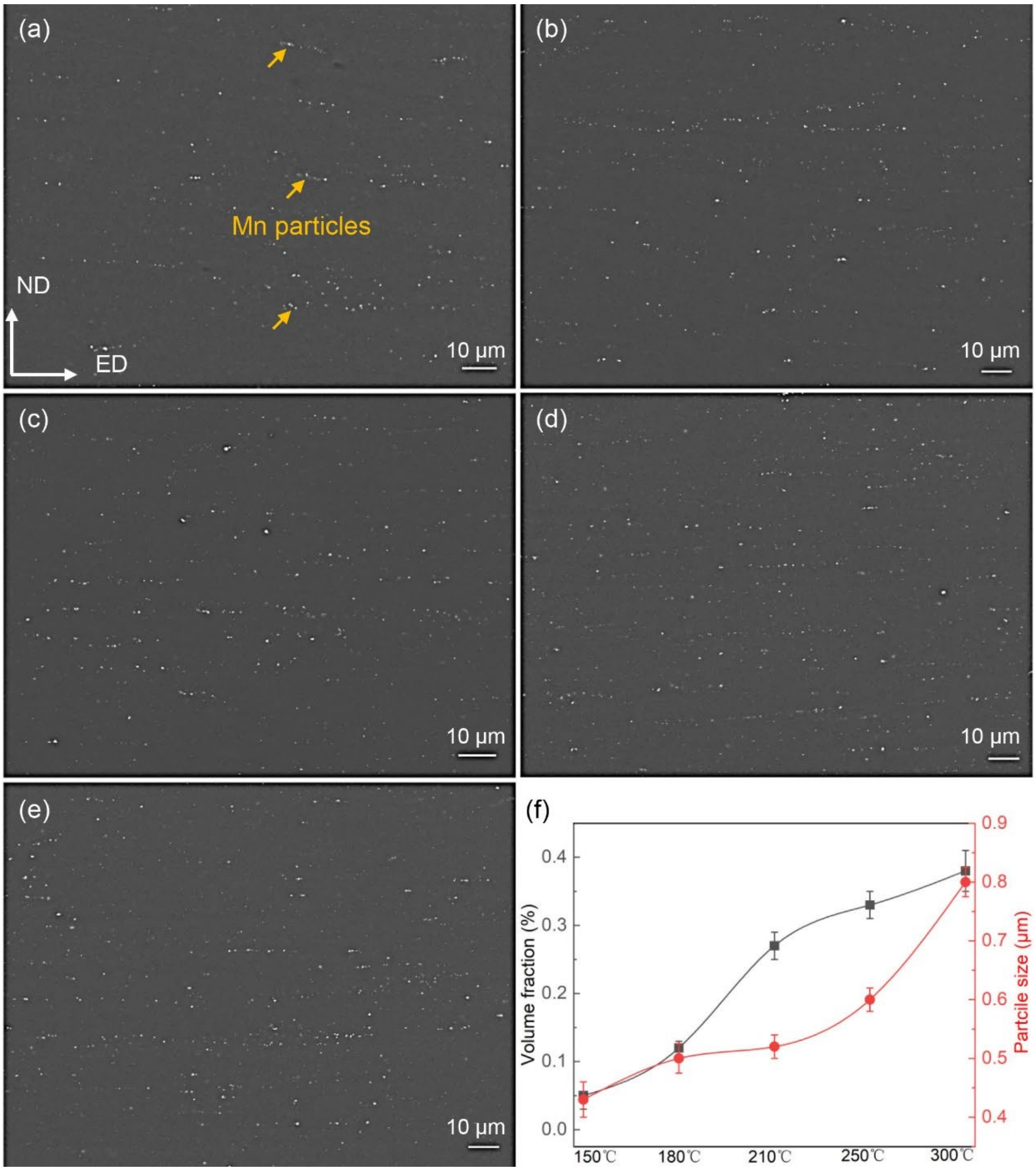

Fig. 3 SEM images of precipitates in M08 alloy extruded at various temperatures: (a) 150 ℃; (b) 180 ℃; (c) 210 ℃; (d) 250 ℃ and (e) 300 ℃.

Fig. 4 displays the TEM images and elemental mappings of the M08-150 and M08-300. A comparative analysis of Fig. 4(a) and Fig. 4(f) reveals that as the extrusion temperature is increased from150 °C to 300 °C, the average size of DRXed grains is increased from 1.4 μm to 5 μm. As shown in Fig. 4(b) and (g), numerous nanosized particles are uniformly distributed within the grain interior and at GBs. According to our previous work [27], the nanosized particles can be identified as α-Mn phase. With the rise in extrusion temperature, the α-Mn particles exhibit a gradual increase in the size from 7±2 nm to 12±3 nm, and the volume fraction is enhanced from 0.18% to

0.36%. Fig. 4(c) and (h) show the HAADF-STEM images of the M08-150 and M08-300 samples, respectively. For the M08-150 sample, noticeable solute segregation of Mn atoms and fine precipitates with approximately 5 nm in size are detectable at GBs. In contrast, as shown in Fig. 4(h)-(j), when the extrusion temperature is increased to 300 °C, the solute segregation of Mn atoms at GBs disappears, and instead a higher volume of α-Mn particles precipitates within the Mg-matrix, demonstrating the influences of extrusion temperature on both precipitation behavior and solute distribution in the Mg-Mn dilute alloy system.

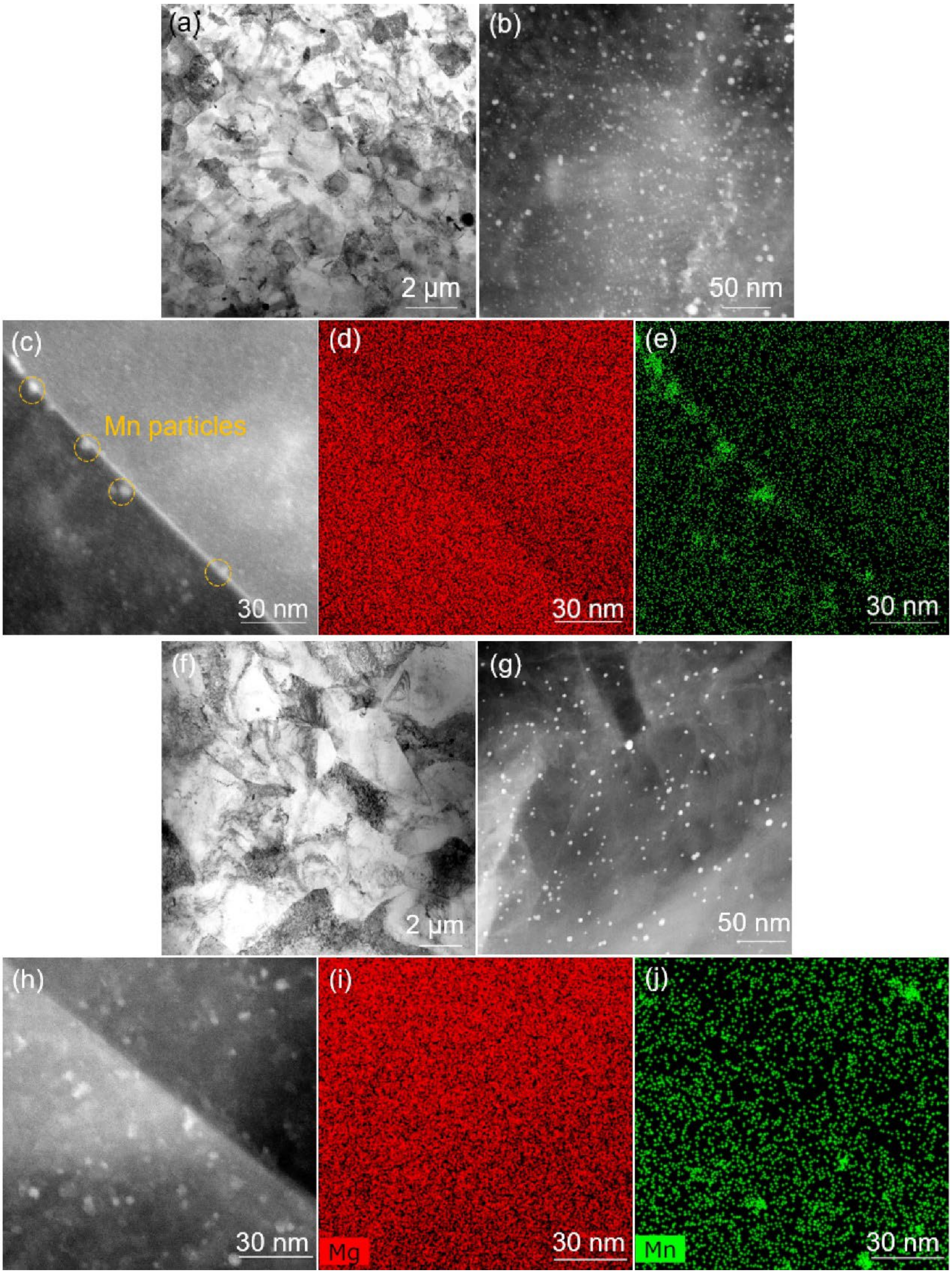

Fig. 4 TEM images of as-extruded M08 samples: Bright field TEM images, precipitates and HAADF-STEM images and elemental mapping distributions of Mg and Mn: (a-e) M08-150 sample; (f-j) M08- 300 sample.

3.2 Mechanical performance of the as-extruded M08 alloy with different DRXed grain sizes

Fig. 5(a) displays the engineering stress-strain curves for M08 samples extruded at various temperatures, while Fig. 5(b) includes digital images of the tensile samples both before and after fracture. The tensile yield strength (TYS), ultimate tensile strength (UTS), and elongation at failure (EL) of the as-extruded M08 samples are listed in Table 1. According to the Hall-Petch relationship, it is commonly observed that a decrease in grain size leads to an increase in yield strength. However, based on Fig. 1 and Fig. 5(c), it is noteworthy that the TYS and UTS of the as-extruded M08 alloy exhibit an abnormally increase with the grain growth of α-Mg matrix. When the extrusion temperature is increased from 150 ℃ to 300 ℃, the TYS of M08 alloy is increased from 117 MPa to 132 MPa, while the EL is reduced from 74$\pm$4 % % to 16$\pm$3 %. Fig. 5(c) shows that the true tensile stress-strain curves and work hardening (WH) behavior of the as-extruded M08 alloy at various extrusion temperatures. Meanwhile, the uniform elongation (ε_u) of the as-extruded M08 alloy experiences a slight increase with the enhanced strain hardening rate at higher extrusion temperatures, but the ε_u value still remains below 6%, indicating that high ductility is primarily attributed to the non-uniform deformation.

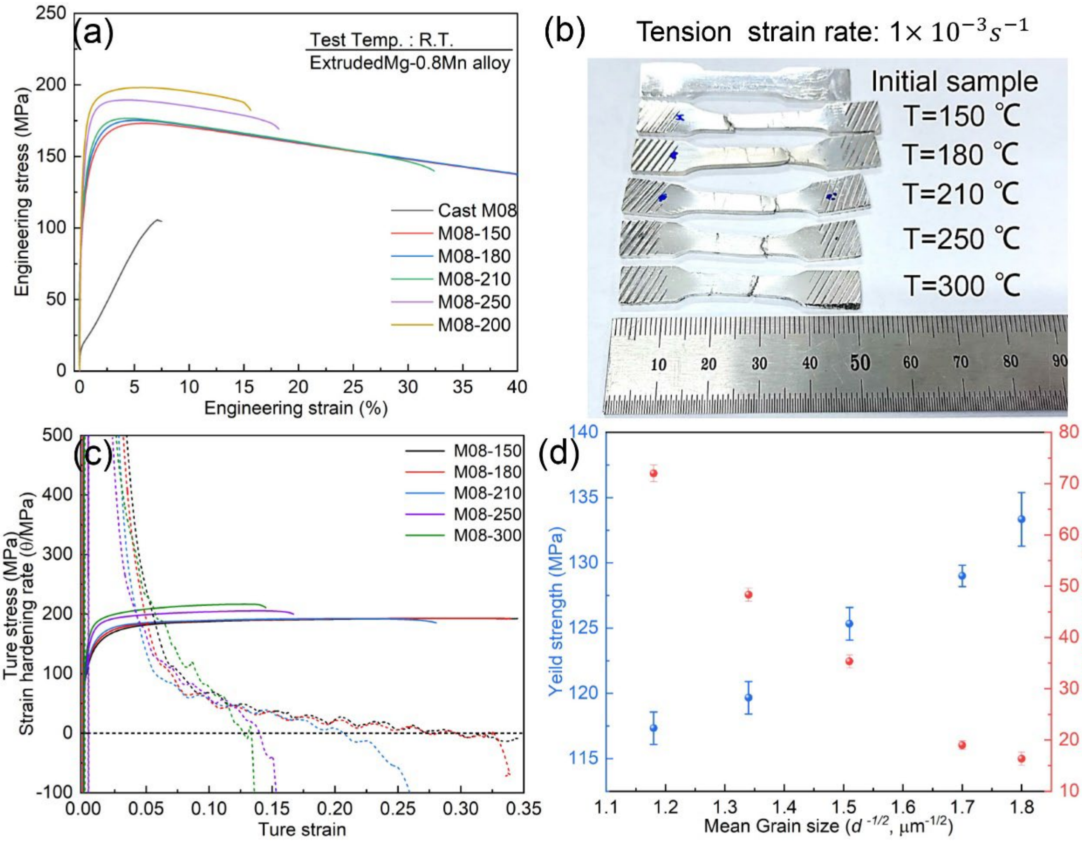

Fig. 5 (a) The tensile engineering stress-strain curves of M08 alloy; (b) Digital photographs of tension samples before and after fracture; (c) Plots of work hardening rate versus tensile true stress - strain curves of as-extruded M08 alloy with varies temperatures; (d) The correlation between yield strength and total elongation with the reciprocal square root of the average DRXed grain size ($d^{-1/2}$).

Table 1. Mechanical performance of M08 alloys subjected to hot extrusion at various temperatures

Extrusion Temperature (T/°C)	DRXed grain size(μm)	f_{DRXed} (%)	TYS (MPa)	UTS (MPa)	ε_u (%)	δ (%)
Cast			10	106		7.6
150	1.4	81.7	117±2	173±2	5.7	74±4
180	1.8	90.8	120±3	175±1	5.1	48±2
210	2.3	95.1	125±2	177±2	4.1	34±3
250	2.9	100	129±1	189±2	4.5	18±2
300	4.9	100	132±4	200±3	5.6	16±3

Fig. 6 presents the SEM images of the fracture morphologies for the M08-150 and M08-300 samples. As shown in Fig. 6(a), the fracture surface of the fine-grained M08-150 sample is predominantly characterized by dense and fine dimples (Zone A), along with a few small cleavage facets (indicated by white arrows). Under uniaxial tensile stress, the fine dimples are generated due to the presence of fine DRXed grains, while the cleavages are originated from the unDRXed regions. As a result, the M08-150 sample exhibits a ductile fracture mode, allowing it to sustain high strain before failure. In contrast, as shown in Fig. 6(c), the large amount of cleavage surfaces and cavities (indicated by red arrow) can be observed in the M08-300 sample. Particularly, Fig. 6 (d) shows numerous cleavages and shallow dimples, indicating that a mixed ductile-brittle fracture occurs during the tension process at room temperature. The similar phenomenon is also found in the pure Mg containing fine grains of ~5.5 μm [30].

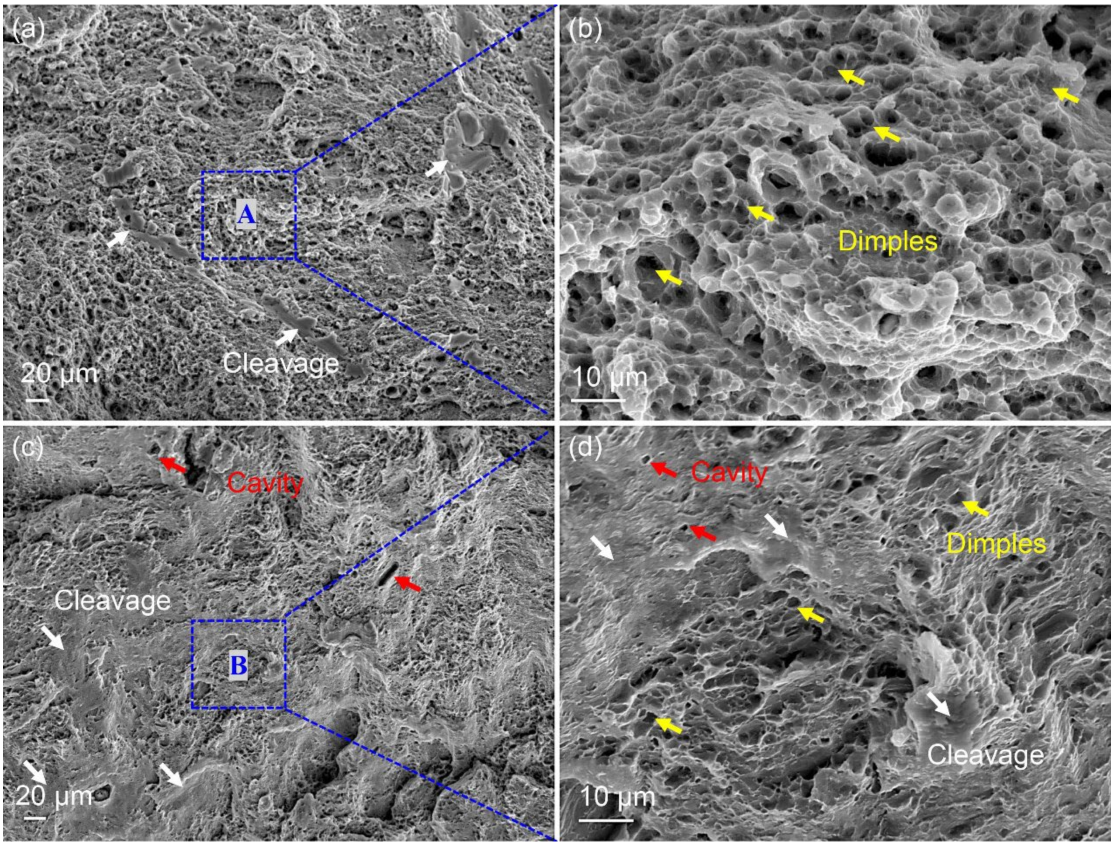

Fig. 6 SEM images of the fracture surface in the as-extruded Mg-0.8Mn samples: (a, b) Fine grained M08 sample extruded at 150 °C and (c, d) Coarse grained M08 sample extruded at 300 °C, respectively.

4. Discussion

4.1 The relationship between the precipitates and Mn segregation at GBs under different extrusion temperatures

Based on the above TEM and SEM observations, solute segregation and fine precipitates can be detected at GBs of M08-150 sample. Nevertheless, upon increasing the extrusion temperature to 300 °C, no Mn atomic segregation at GBs is observed, whereas the Mn particles with approximately 12 nm in diameter appear within the grain interior of α-Mg matrix. Figs. 7(a-d) show the TEM images of the homogenized M08 alloy. It presents only a small number of Mn particles with approximately 70 nm in size, without any detectable nano-sized precipitates. To better visualize the dynamic precipitation of Mn particles during the extrusion process, the homogenized M08 alloy was subjected to a pre-extrusion treatment at 150 °C for 20 min, as shown in Figs. 7(e-h). It can be found that the microstructure is composed of long rod-shaped Mn particles with the length of up to 200 nm, but with no evidence of nano-sized Mn particles. This observation can be attributed to the significant density difference between the Mg matrix and Mn particles at room temperature. When the Mn particles precipitate in the Mg matrix, they can induce significant tensile stress, which thermodynamically promotes the occurrence of phase transformation. To minimize strain energy and reduce tensile stress, Mn particles tend to adopt morphologies with higher axial ratios [31]. However, substantial compressive stress is produced by the density difference between the Mn particles and the Mg matrix, which can partially alleviate the tensile stress. As illustrated in Fig. 4, the Mn precipitates initially form rod-shaped particles, which subsequently become spherical to minimize the contact energy during extrusion. Furthermore, due to the short holding time of the M08 billets at prior to extrusion, the Mn solutes cannot be fully dissolved in the supersaturated Mg matrix. As shown in Fig. 4, additional precipitation of finer Mn particles occurs during the hot extrusion. Besides, the extrusion-induced defects can provide new nucleation sites to facilitate the precipitation of fine particles [32].

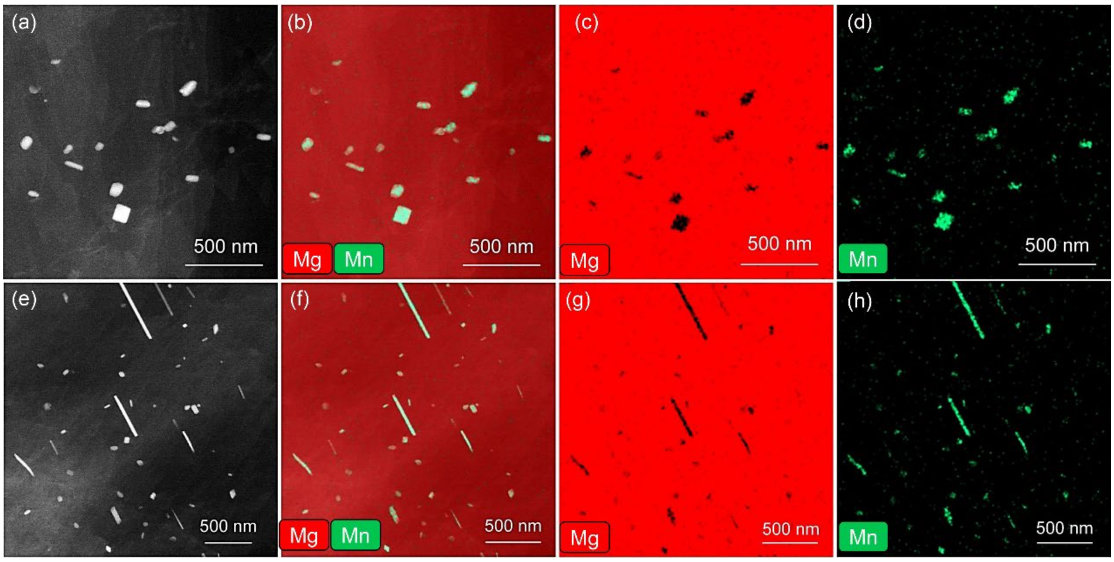

Fig. 7 TEM images and mappings of M08 alloy: (a-d) homogenized; (e-h) Pre-treated before extrusion

The atomic radius of Mn (0.15 nm) is smaller than that of Mg (0.16 nm), and the solute atom mismatch of 6.25 % can provide the driving force for the Mn segregation at GBs [33]. Generally, the trend of GB segregation is primarily governed by the Gibbs free energy associated with GB segregation [34]. According to the traditional Langmuir-McLean (L-M) equation [35], the solute atom distribution can be represented by the following Eq. (1).

$$\frac{X_{GB}}{1-X_{GB}}=\frac{X_i}{1-X_i}\exp\left(-\frac{\Delta G_{seg}}{RT}\right), \quad (1),$$

where X_{GB} and X_i are the molar grain boundary occupation fraction and the molar concentration of i atom in the Mg-matrix, respectively, and ΔG_{seg} is the free energy of segregation. According to Eq. (1), it can be deduced that an increase in the extrusion temperature can induce the decreased Mn atomic segregation at GBs. This reduction may diminish the solute drag effect on the GB mobility, leading to an unavoidable grain growth with the increase of extrusion temperature [36]. The precipitation of Mn particles in Mg-Mn alloys is regarded as a rapid process. Therefore, an elevated extrusion temperature can facilitate the generation of Mn particles within the α-Mg grains.

4.2 Strengthening mechanisms of M08 samples extruded at different temperatures

As shown in Fig. 8(a), the SRS exponent (m-value) of the M08 alloy extruded at various temperatures can be determined by the change in indentation depth with time. The connection between stress σ and strain rate $\dot{\varepsilon}$ during the creep test is described by the traditional Tabor relation, as illustrated in Eq. (2) [37].

$$\sigma = b(\dot{\varepsilon})^m \quad (2),$$

where σ is uniaxial flow stress, $\dot{\varepsilon}$ is uniaxial strain rate, b is material-related constant, and m is SRS exponent. The actual effective strain rate ($\dot{\varepsilon}_{eff}$) is defined as the instantaneous rate of the decrease of indentation during the indentation process divided by the indentation depth, which can be expressed as [38]:

$$\dot{\varepsilon}_{eff} = A\times\dot{\varepsilon} = A\times\left(\frac{1}{h}\right)\left(\frac{dh}{dt}\right) \quad (3)$$

where A is a constant of 0.1[39,40], h is the indentation depth, t is the effective creep time. As presented in Fig. 8(b), the m-value is determined as 0.16, 0.15, 0.1, 0.09 and 0.006 for the M08 alloy extruded at 150 °C, 180 °C, 210 °C, 250°C and 300 °C, respectively. The grain growth occurs with the increase of extrusion temperature, which subsequently diminishes the role of GBS in the overall deformation process. As a result, dislocation slip becomes the dominated deformation mode for the M08-300 sample.

It is noteworthy that the inverse relationship between grain size and YS is primarily attributed to changes in the deformation mechanism [41]. In present work, GBS plays a dominant role in the deformation mode of M08 alloy extruded at 150 °C. The nanoindentation creep experiments confirmed an m-value of 0.15, indicating the effect of grain boundary softening. Conversely, in the M08 alloy extruded at 300 °C, dislocation slip becomes the primary deformation mechanism. The low m-value in this case also suggests the presence of grain boundary strengthening, which can explain the observed increase in YS with grain coarsening.

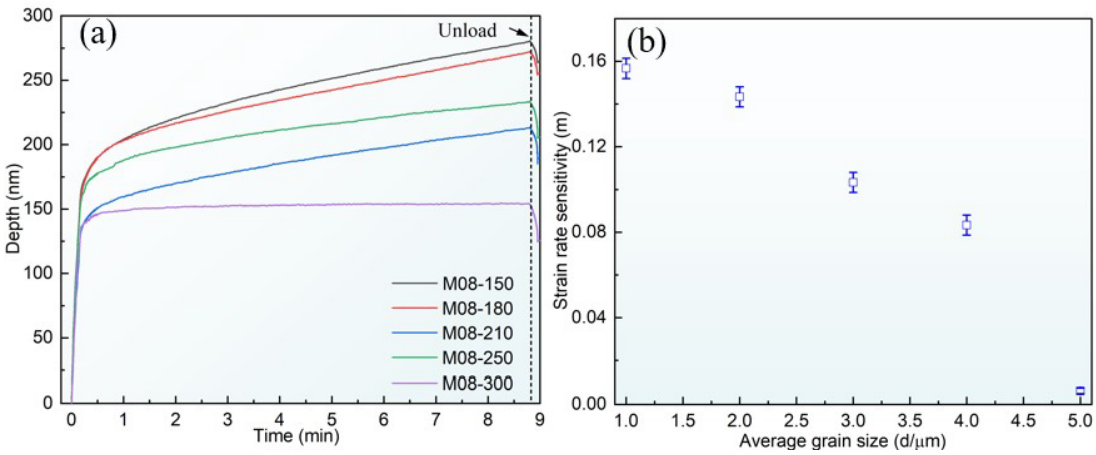

Fig. 8 (a) The variation of indentation depth as a function of time in the M08 alloy extruded at different temperatures; (b) Plots of SRS (*m*-value) against the average DRXed grain size.

The strengthening mechanisms of the M08-150 and M08-300 samples with distinct microstructure characteristics are discussed as follows. The TYS of the Mg-Mn alloy can be estimated by *Eq.* (5),

$$\sigma_{tys} = \sigma_0 + \sigma_{gb} + \sigma_p + \sigma_{dis} \tag{5}$$

where σ_0 is solid solution strengthening [42], σ_{gb} is GB strengthening, σ_p is particle strengthening, and σ_{dis} is dislocation strengthening.

It is generally accepted that the σ_0 is approximately equivalent to the yield strength of as-cast M08 alloy (~10 MPa). As reported, for pure Mg containing fine grains of 0.65 μm, and the GBS is the dominant deformation mode. The critical shear stress needed for GBS is significantly lower than that required for basal slip [43]. Therefore, the contribution of σ_{gb} in the fine-grained DRXed regions to TYS of M08-150 sample can be neglected.

The KAM map obtained from EBSD can be used to quantitatively calculate the geometric necessary dislocation (GND) density, providing insight into the homogenization of plastic deformation. Higher KAM values correspond to greater plastic deformation or higher defect densities [44]. Based on the EBSD analysis, the KAM values in the DRXed and un-DRXed regions are 0.03° and 0.016°, respectively (see Fig 8). According to the *Eq.* (6) [45], the density of GND in the unDRXed and DRXed regions of the M08-150 sample can be determined as 3×10^{14}m^{-2} and

$2.29\times10^{14}m^{-2}$, respectively.

$$\rho_{GND}=\frac{2\overline{KAM}}{\mu b}, \tag{6}$$

where μ is the EBSD step size of 0.4 μm and b is the Berger's vector (0.32 nm). The σ_{GND} can be calculated by *Eq.* (7) [46],

$$\sigma_{GND}= f_{DRXed}M\alpha Gb\sqrt{\rho_{GND}}+(1-f_{DRXed})M\alpha Gb\sqrt{\rho_{GND}} \tag{7}$$

where the value of M for DRXed regions with strong texture is 2.5 [47], α is a constant (~0.20); G is shear modulus (16.6 GPa), b is the Burger's vector (0.32 nm), f_{DRXed} is the volume fraction of DRXed (80.7 %). The σ_{GND} values of the DRXed and unDRXed regions are determined to be 33 MPa and 12 MPa, respectively, and thereby the total σ_{GND} is estimated to be 45 MPa.

The contribution of σ_p can be estimated by *Eq.* (8) [48]

$$\sigma_p=\frac{MGb}{2\pi\sqrt{1-v}(\frac{0.779}{\sqrt{fp}}-0.785)d_p}\ln\frac{0.785d_p}{b}, \tag{8}$$

where G is shearing modulus, v is Poisson's ratio (0.3), b is Burger's vector, d_p is the average diameter of the spherical precipitates, f_p is the volume fraction of the precipitates. Two distinct precipitate sizes are present, i.e. 300 nm and 7 nm in diameter. The respective volume fractions for the larger and smaller precipitates are 0.05% and 0.18%. The σ_p values in the M08-150 sample with fine and large precipitates are calculated as 2 MPa and 58 MPa, respectively. Accordingly, the precipitation strengthening effect contributes an increment of 60 MPa to the M08-150 sample. Hence, based on Eq. (5), the yield strength for M08-150 sample is calculated to be ~115 MPa.

Since dislocation slip is the main deformation mechanism in the M08-300 sample with the fully DRXed grains of 4.9 μm, the contribution of GB strengthening σ_{gb} for the M08-300 sample can be calculated using Eq. (10) [46].

$$\sigma_{gb}= k\cdot d^{-1/2} \tag{10}$$

where k is the Hall-Petch coefficient taken as ~ 157 MPa·μm$^{-1/2}$ [49] (Here we choose the k-value of extruded pure Mg with similar mechanical properties and grain size between 4-63 μm). The σ_{gb} in the M08-300 sample is calculated to be 70 MPa. According to the Eq. (8), the contributions of two types of large-sized (800 nm, 0.34 %) and small-sized (15 nm, 0.36%) precipitates are 2 MPa and 50 MPa, respectively. It can be seen from Fig. 9 (c) and (f) that the KAM value of the M08-300 sample is 0.016 °, and the ρ_{GND} calculated by *Eq.* (6) is about $1.02\times10^{14}m^{-2}$. Thus, the σ_{dis} of M08-300 sample is calculated to be 26 MPa. According to the Eq. (5), the TYS of M08-300 sample is estimated as ~158 MPa. Although the calculated TYS is higher than the experimentally measured TYS, both exhibit a consistent variation trend. The discrepancy between the calculated and measured strengths may be attributed to the model selection and potential measurement errors.

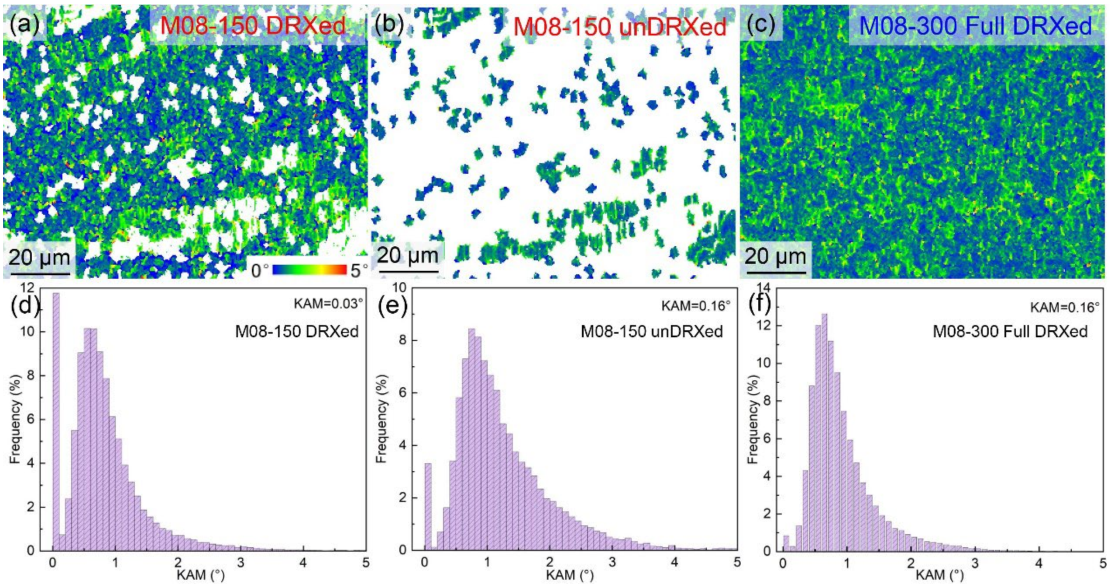

Fig. 9 KAM maps of the as-extruded M08 samples: (a,d) DRXed regions of M08-150 sample; (b,e) unDRXed regions of M08-150 sample; (c,f) Full DRXed regions of M08-300 sample.

Table 2 The strengthening contributions of M08-150 and M08-300 samples

Sample	σ_p (MPa)	σ_{dis} (MPa)	σ_0 (MPa)	σ_{gb} (MPa)	Calculated YS (MPa)	Measured YS (MPa)
M08-150	60	46	10	-	118	117
M08-300	52	26	10	73	158	132

It is noteworthy that the TYS of the M08 sample is increased with the DRXed grain growth, which is contrary to the Hall-Petch relationship. This is probably associated with a transition in the plastic deformation mechanism, and an analogous increase in the TYS has been documented in pure Mg as the grain size was increased from 2.4 μm to 93 nm [50]. Based the nanoindentation creep experimental results as shown in Fig. 9, the *m*-value is dependence of the extrusion temperature. It is found that the *m*-value for the full DRXed M08-210 alloy is 0.1, while the m-value for the M08-300 alloy is only 0.009. The contribution of GBS was calculated using the roughness in the x-z direction of AFM. As shown in Fig. 10, the contribution of GBS to plastic deformation in the M08-150 sample is 35 %, whereas this contribution is reduced to 15% in the M08-210 sample. A lower *m*-value suggests that plastic deformation is primarily governed by dislocation slip [42]. This could be derived from the transition of plastic deformation mechanism when the extrusion was performed at 210 °C. In the M08-300 sample, due to the small *m*-value (0.009), dislocation slip accounts for a significant contribution in deformation. The dominance of GBS in plastic deformation is evidenced by a higher *m*-value. However, when the extrusion temperature exceeds 210 ℃, the influence of GBS is diminished, while the contribution of dislocation slip becomes more pronounced. In particular, when the extrusion temperature is increased, Mn particles are precipitated [43]. Therefore, as the grain growth occurs with the rise in extrusion temperature, the contribution of GBS is diminished, while the significance of dislocation slip becomes more prominent.

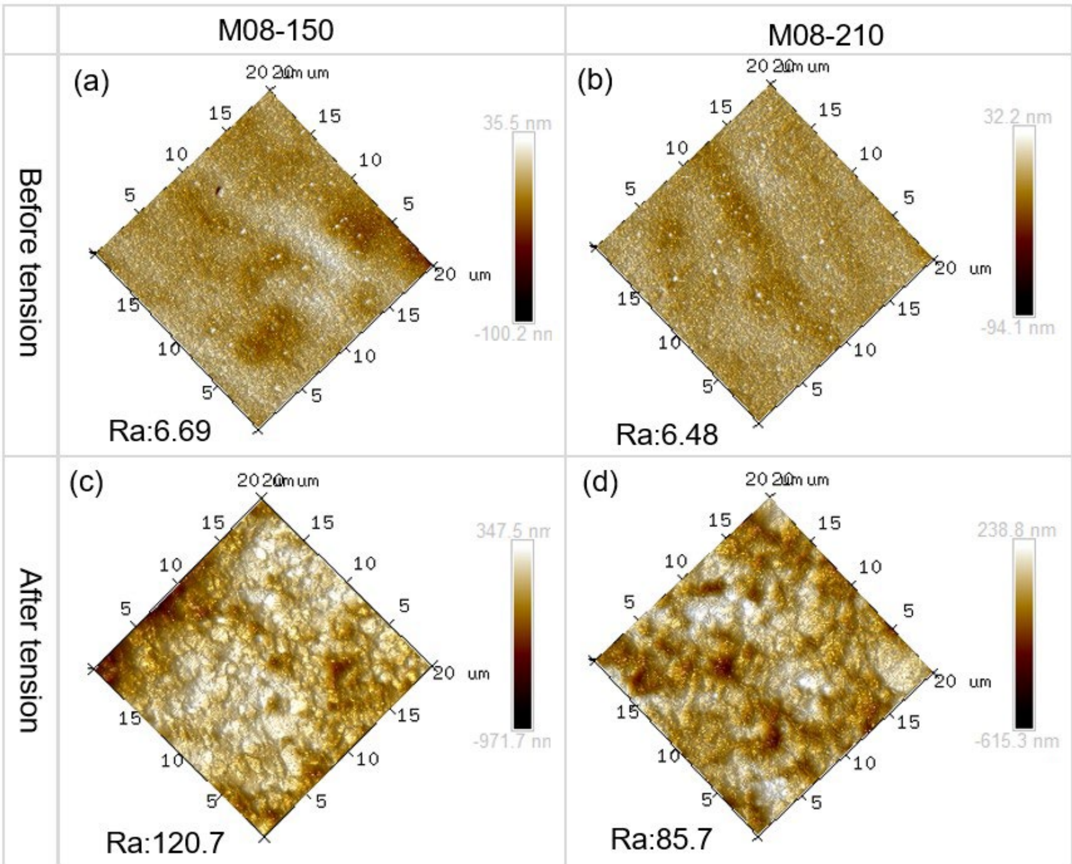

Fig. 10 AFM images illustrating the surface roughness of as-extruded M08-150 and M08-210 samples: (a) and (b) Surface roughness images prior to the tensile test; (c) and (d) Surface roughness images after tensile test.

4.3 Effect of DRXed grain size on work hardening in as-extruded M08 alloys

Fig. 11 shows the impact of various DRXed grain sizes on work hardening rate

(θ). It is evident that as the DRXed grain size is increased from 1.4 to 4.9 μm, and there is a corresponding rise in the work hardening rate. The influence of grain size was also observed in the as-rolled AZ31 alloys in relation to the change in the slip system [26]. As reported, the deformation mechanism of pure Mg containing fine grains of 50 nm was dominated by GBS [51]. When subjected to external stress, fine grains undergo GBS, the dislocations are not easily accumulated within the grains. In contrast, for the coarse-grained M08-300 alloy, the dislocation slip becomes the main deformation mechanism.

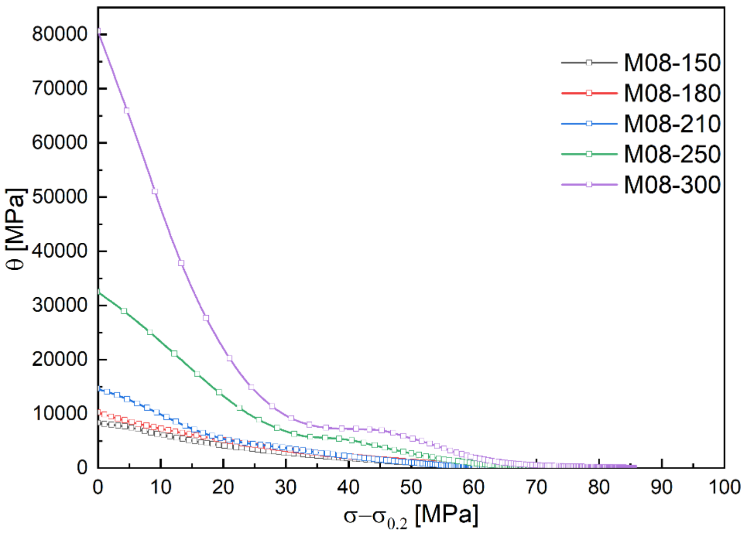

Fig. 11 Effect of the DRXed grain size on the WH behavior of the as-extruded M08 alloy: a plot of θ against (σ-$\sigma_{0.2}$).

To elucidate the association between DRXed grain size and the work hardening rate (θ), Fig. 12 presents the volume fractions of LAGBs for the M08-150 and M08-300 alloys before and after tension test. The M08-150 and M08-300 samples are selected as the typical representatives on work hardening of the dislocation slip and GBS, respectively. Since the two typical alloys continue to have a basal fiber texture before and after tension, the effect of the texture on θ is not primarily considered. By comparing the EBSD-IPF results of M08-150 samples before tension and after fracture in Figs. 12(a) and (c), an increase in the gray line is visually observed. The dislocation density in the unDRXed area is significantly increased, and the volume fraction of the LAGBs is increased from 17.7% to 20.7%. As shown in Figs. 12(b) and 11(d), the dislocation density of the M08-300 samples reaches $1.71\times10^{14}m^{-2}$, and the volume fraction of LAGBs is significantly enhanced from 26.6 % to 32.4%. Both the elongated unDRXed grains and micron-sized DRXed grains are favorable for dislocation storage. Therefore, grain size has a profound impact on work hardening rate. The grain size of as-extruded M08 sample is positively correlated with the work hardening rate, and the M08-300 sample with coarse grains is more prone to dislocation stored, resulting in a higher work hardening rate [52].

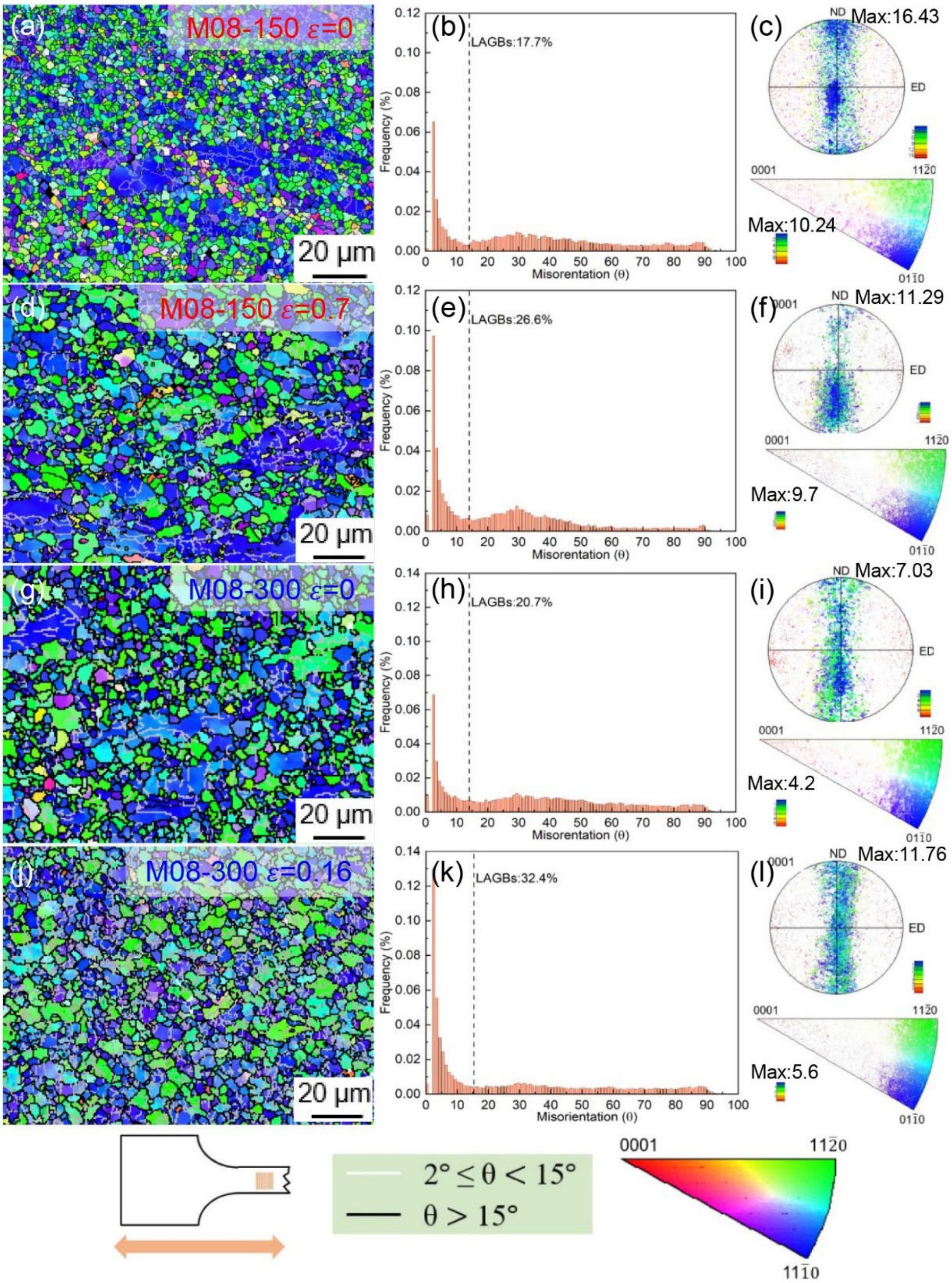

Fig. 12 EBSD-IPF, small angle grain boundary volume fractions and full pole and reverse pole figures: (a-c) M08-150 samples before tension; (d-f) M08-150 samples after fracture; (g-i) M08-

300 samples before tension; (j-l) M08-300 samples after fracture.

Conclusions

In present work, the impacts of grain size on mechanical behavior and work hardening performance of the as-extruded Mg-0.8Mn (wt.%) (M08) samples during room temperature tensile testing are systematically explored. The primary findings can be summarized as follows:

1. The M08 alloy possesses a bimodal microstructure characterized by elongated undynamically recrystallized (unDRXed) grains and fine dynamically recrystallized (DRXed) grains when extruded below 210 °C. In contrast, a full DRXed microstructure is obtained when extruded at the temperature above 210 °C. Moreover, an increase in the extrusion temperature from 150 ºC to 300 ºC can bring about the growth of DRXed grains from 1.4 μm to 4.9 μm.

2. As the extrusion temperature is increased, the M08 alloy demonstrates a corresponding rise in tensile yield strength from 117 MPa to 140 MPa, accompanied with a reduced failure elongation from 74% to 16%. These changes in mechanical properties are predominantly ascribed to the reduced occurrence of GBS during plastic deformation.

3. The DRXed grain size has notable influences on the work hardening rate. The as-extruded M08 alloy that possesses coarser grains demonstrates a more pronounced work hardening rate as compared to those with finer grains. This phenomenon is mainly due to the fact that numerous dislocations can be stored within the coarse grains of the as-extruded M08 alloy, and dislocation slip is identified as the dominant mechanism for plastic deformation.

Acknowledgments

This work is supported by National Key Research and Development Program of China (No. 2022YFE0109600), and National Natural Science Foundation of China (No. 51971076, No. U21A2047 and No. 51771062), the National Research Foundation of Korea (NRF) grant funded by the Korea government (MSIP) (NRF-2021R1A2C3006662, NRF-2022R1A5A1030054). Mr. Chongchao Li is supported by the China Scholarship Council (CSC, No.202206120129).

References

[1] A.A. Kaya, A Review on Developments in Magnesium Alloys, Front. Mater. 7 (2020) 1–26.

[2] Y. Cui, H. Bian, Y. Li, Y. Zhao, K. Aoyagi, A. Chiba, Impacts of pre-strain on twin boundary mobility of magnesium, J. Alloys Compd. 816 (2020) 152496.

[3] Y. Yang, X. Xiong, J. Chen, X. Peng, D. Chen, F. Pan, Research advances of magnesium and magnesium alloys worldwide in 2022, J. Magnes. Alloy. 11 (2023) 2611–2654.

[4] H. Wang, D.T. Zhang, C. Qiu, W.W. Zhang, D.L. Chen, Materials Science & Engineering A Achieving superior mechanical properties in a low-alloyed magnesium alloy via low-temperature extrusion, Mater. Sci. Eng. A. 851 (2022) 143611.

[5] Z. Zeng, N. Stanford, C.H.J. Davies, J.F. Nie, N. Birbilis, Magnesium extrusion alloys: a review of developments and prospects, Int. Mater. Rev. 64 (2019) 27–62.

[6] Y. niu Li, K. kun Deng, C. ju Wang, K. bo Nie, Q. xin Shi, P. cheng Tian, G.W. Zhang, Effect of final rolling deformation on microstructure, work hardening and softening behavior of Mg-8Li-3Al-0.3Si alloys, J. Alloys Compd. 990 (2024) 174427.

[7] F. Zhao, J. Xie, Y. Zhu, Q. Liu, T. Ye, L. Chen, T. Suo, K. Wang, T. Wang, Q. Wang, A novel dynamic extrusion for microstructure tailoring and evading strength-ductility trade-off in AZ31 magnesium alloy, J. Alloys Compd. 870 (2021) 159411.

[8] D. Zhao, G. Li, P. Li, J. Zhou, K. Cheng, Y. Liu, Y. Yang, J. Duan, R. Ghomashchi, X. Wang, A comparative study on the microstructures and mechanical properties of the Mg-xCa/Mn/Ce alloys and pure Mg, Mater. Sci. Eng. A. 803 (2021) 140508.

[9] P. Peng, A. Tang, B. Wang, S. Zhou, J. She, Achieving superior combination of yield strength and ductility in Mg e Mn e Al alloys via ultrafine grain structure, J. Mater. Res. Technol. 15 (2021) 1252–1265.

[10] Y. Li, M. Wang, J. Cai, P. Ma, X. Zhao, Z. Li, Fabrication of high strength-ductility Mg-3.8Al-1.1Sn-0.4Ca alloy via differential-thermal asymmetric extrusion, J. Alloys Compd. 1002 (2024) 175182.

[11] W. Xu, S. Ouyang, L. Deng, G. Zhu, X. Chen, F. Pan, Enhanced mechanical properties and electromagnetic interference shielding effectiveness in Mg-6Zn-1Y-1La-0.5Zr alloy sheet by hot deformation, J. Alloys Compd. 1003 (2024) 175716.

[12] Z. Song, R. Niu, X. Cui, E. V. Bobruk, M.Y. Murashkin, N.A. Enikeev, J. Gu, M. Song, V. Bhatia, S.P. Ringer, R.Z. Valiev, X. Liao, Mechanism of room-temperature superplasticity in ultrafine-grained Al–Zn alloys, Acta Mater. 246 (2023) 1–12.

[13] Z. Zeng, J.F. Nie, S.W. Xu, C.H.J. Davies, N. Birbilis, Super-formable pure magnesium at room temperature, Nat. Commun. 8 (2017) 1–6.

[14] H. Somekawa, D.A. Basha, A. Singh, Room temperature grain boundary sliding

behavior of fine-grained Mg-Mn alloys, Mater. Sci. Eng. A. 730 (2018) 355–362.
[15] H. Somekawa, A. Singh, Superior room temperature ductility of magnesium dilute binary alloy via grain boundary sliding, Scr. Mater. 150 (2018) 26–30.
[16] H. Somekawa, D. Egusa, E. Abe, Grain boundary plasticity in solid solution Mg–Li binary alloy, Mater. Sci. Eng. A. 790 (2020) 139705.
[17] I.S. Golovin, V. V. Palacheva, J. Cifre, C.C. Li, X.G. Qiao, M.Y. Zheng, Anelasticity of Mg-Mn and Mg-Gd alloys, J. Alloys Compd. 995 (2024) 174777.
[18] H. Somekawa, A. Singh, T. Mukai, T. Inoue, Effect of alloying elements on room temperature tensile ductility in magnesium alloys, Philos. Mag. 96 (2016) 2671–2685.
[19] Z. Zeng, M. Zhou, P. Lynch, F. Mompiou, Q. Gu, M. Esmaily, Y. Yan, Y. Qiu, S. Xu, H. Fujii, C. Davies, J.F. Nie, N. Birbilis, Deformation modes during room temperature tension of fine-grained pure magnesium, Acta Mater. 206 (2021) 116648.
[20] H. Somekawa, A. Kinoshita, A. Kato, Great room temperature stretch formability of fine-grained Mg-Mn alloy, Mater. Sci. Eng. A. 697 (2017) 217–223.
[21] K. Edalati, T. Masuda, M. Arita, M. Furui, X. Sauvage, Z. Horita, R.Z. Valiev, Room-Temperature Superplasticity in an Ultrafine-Grained Magnesium Alloy, Sci. Rep. 7 (2017) 1–9.
[22] M. li Hou, K. kun Deng, C. ju Wang, K. bo Nie, Q. xin Shi, The balance between work hardening and softening behaviors of Mg-xZn-1Gd-0.2Ca-0.1Zr alloys influenced by trace Zn addition, J. Alloys Compd. 969 (2023) 172379.
[23] B. Zhou, T. Zhu, H. Jia, Z. Ma, T. Hao, J. Wang, X. Zeng, Revealing the weak work-hardening behavior in aged Mg–RE alloys: A synchrotron radiation diffraction study, J. Alloys Compd. 947 (2023) 169705.
[24] J. Zhao, B. Jiang, Y. Yuan, A. Tang, Influence of Zn addition on the microstructure, tensile properties and work-hardening behavior of Mg-1Gd alloy, Mater. Sci. Eng. A. 772(2020)138779.
[25] Z. Wang, H. Ding, Z. Xiao, C. Yang, C. Xiang, Experimental investigation on the mechanical properties and strain rate sensitivity of Mg–Al–Ca–Mn alloy under various strain rates, Mater. Sci. Eng. A. 826 (2021) 141997.
[26] J. Koike, T. Kobayashi, T. Mukai, H. Watanabe, M. Suzuki, K. Maruyama, K. Higashi, The activity of non-basal slip systems and dynamic recovery at room temperature in fine-grained AZ31B magnesium alloys, Acta Mater. 51 (2003) 2055–2065.
[27] C.C. Li, Z.H. Xia, X.G. Qiao, I.S. Golovin, M.Y. Zheng, Superior ductility Mg-Mn extrusion alloys at room temperature obtained by controlling Mn content, Mater. Sci. Eng. A. 869 (2023) 144508.
[28] ASTM E8-E8M-16A. Standard test method for tension testing of metecillc materails, 2016.
[29] H. Borkar, M. Pekguleryuz, Effect of Extrusion Parameters on Texture and Microstructure Evolution of Extruded Mg-1 pctMn and Mg-1 pctMn-Sr Alloys, Metall. Mater. Trans. A Phys. Metall. Mater. Sci. 46 (2015) 488–495.

[30] K. Wei, R. Hu, D. Yin, L. Xiao, S. Pang, Y. Cao, H. Zhou, Y. Zhao, Y. Zhu, Grain size effect on tensile properties and slip systems of pure magnesium, Acta Mater. 206 (2021) 116604.

[31] M. Kato, Crystallography and energetics of second phases and interfaces, Mater. Trans. 59 (2018) 509–517.

[32] Y.F. Liu, X.G. Qiao, Z.T. Li, Z.H. Xia, M.Y. Zheng, Effect of nano-precipitation on thermal conductivity and mechanical properties of Mg-2Mn-xLa alloys during hot extrusion, J. Alloys Compd. 830 (2020) 154570.

[33] W. Sun, Y. He, X. Qiao, X. Zhao, H. Chen, N. Gao, M.J. Starink, M. Zheng, Exceptional thermal stability and enhanced hardness in a nanostructured Mg-Gd-Y-Zn-Zr alloy processed by high pressure torsion, J. Magnes. Alloy. (2022). 003.

[34] C. Wang, J. Wang, D. Ma, S. Zhu, L. Wang, S. Guan, First-principles studies on structure stability, segregation, and work function of Mg doped with metal elements, Int. J. Quantum Chem. 121 (2021) 1–9.

[35] W.T. Sun, X.G. Qiao, M.Y. Zheng, C. Xu, S. Kamado, X.J. Zhao, H.W. Chen, N. Gao, M.J. Starink, Altered ageing behaviour of a nanostructured Mg-8.2Gd-3.8Y-1.0Zn-0.4Zr alloy processed by high pressure torsion, Acta Mater. 151 (2018) 260–270.

[36] Z.R. Zeng, Y.M. Zhu, R.L. Liu, S.W. Xu, C.H.J. Davies, J.F. Nie, N. Birbilis, Achieving exceptionally high strength in Mg–3Al–1Zn-0.3Mn extrusions via suppressing intergranular deformation, Acta Mater. 160 (2018) 97–108.

[37] H. Somekawa, T. Mukai, Nanoindentation creep behavior of grain boundary in pure magnesium, Philos. Mag. Lett. 90 (2010) 883–890.

[38] M.J. Mayo, W.D. Nix, A micro-indentation study of superplasticity in Pb, Sn, and Sn-38 wt% Pb, Acta Metall. 36 (1988) 2183–2192.

[39] E. Song, M.T. Andani, A. Misra, Investigation of grain size and geometrically necessary dislocation density dependence of flow stress in Mg-4Al by using nanoindentation, Acta Mater. 265 (2024) 119633.

[40] S.Y. Yan, Z.J. Wang, Z.W. Shan, Abnormally enhanced displacement burst at elevated temperatures of AZ31 magnesium alloy during nanoindentation, J. Mater. Sci. Technol. 211 (2025) 171–178.

[41] R. Ni, S. Hua, S. Huang, Y. Zeng, Y. Chai, H. Zhou, J. Zheng, D. Yin, Effect of grain size on tensile behavior and the underlying deformation modes in a Mg-5Y sheet, J. Alloys Compd. 1008 (2024) 176570.

[42] H. Pan, G. Qin, Y. Huang, Y. Ren, X. Sha, X. Han, Z.Q. Liu, C. Li, X. Wu, H. Chen, C. He, L. Chai, Y. Wang, J. feng Nie, Development of low-alloyed and rare-earth-free magnesium alloys having ultra-high strength, Acta Mater. 149 (2018) 350–363.

[43] R. Zheng, J.P. Du, S. Gao, H. Somekawa, S. Ogata, N. Tsuji, Transition of dominant deformation mode in bulk polycrystalline pure Mg by ultra-grain refinement down to sub-micrometer, Acta Mater. 198 (2020) 35–46.

[44] X. Qi, Y. Li, X. Zeng, Role of prismatic<a>dislocations in sub-zero temperature deformation of Mg-Gd-Y-Zr alloy, J. Alloys Compd. 960 (2023). 170803.

[45] Z. Yan, D. Wang, X. He, W. Wang, H. Zhang, P. Dong, C. Li, Y. Li, J. Zhou, Z. Liu, L. Sun, Deformation behaviors and cyclic strength assessment of AZ31B magnesium alloy based on steady ratcheting effect, Mater. Sci. Eng. A. 723 (2018) 212–220.

[46] P. Luo, D.T. McDonald, W. Xu, S. Palanisamy, M.S. Dargusch, K. Xia, A modified Hall-Petch relationship in ultrafine-grained titanium recycled from chips by equal channel angular pressing, Scr. Mater. 66 (2012) 785–788.

[47] Q. Wang, H. Zhai, L. Liu, Z. Jin, L. Zhao, J. He, B. Jiang, Exploiting an as-extruded fine-grained Mg-Bi-Mn alloy with strength-ductility synergy via dilute Zn addition, J. Alloys Compd. 924 (2022) 166337.

[48] J.F. Nie, Effects of precipitate shape and orientation on dispersion strengthening in magnesium alloys, Scr. Mater. 48 (2003) 1009–1015.

[49] S.M. Razavi, D.C. Foley, I. Karaman, K.T. Hartwig, O. Duygulu, L.J. Kecskes, S.N. Mathaudhu, V.H. Hammond, Effect of grain size on prismatic slip in Mg-3Al-1Zn alloy, Scr. Mater. 67 (2012) 439–442.

[50] R. Ren, J. Fan, B. Wang, Q. Zhang, W. Li, H. Dong, Hall-Petch relationship and deformation mechanism of pure Mg at room temperature, J. Alloys Compd. 920 (2022) 165924.

[51] S. Hwang, C. Nishimura, P.G. McCormick, Deformation mechanism of nanocrystalline magnesium in compression, Scr. Mater. 44 (2001) 1507–1511.

[52] M.S. Hasan, R. Lee, W. Xu, Deformation nanomechanics and dislocation quantification at the atomic scale in nanocrystalline magnesium, J. Magnes. Alloy. 8 (2020) 1296–1303.